對活躍星系 X 射線噴流的多波段研究

黃貞媛[a]、陳林文[b]

[a.] 中央研究院天文及天文物理研究所

[b.] 國立台灣師範大學地球科學系

摘要

利用多波段的觀測數據，我們進行一系列對活躍星系中高能輻射噴流本質的探討。經由這幾年的研究，產生這些 X 射線噴流的主要輻射機制通常可歸結成同步加速輻射（synchrotron），逆康普敦散射宇宙微波背景光子(IC/CMB)，或同步自康普敦散射(SSC)。然而目前對所有已觀測的 X 射線噴流並無一致的解釋，同時不同輻射模型所預測的物理環境也常隨之變化。爲了有系統地檢驗已知的高能噴流，以及更廣泛地探討 X 射線噴流的起源，我們利用從電波波段到 X 射線的觀測數據，加上一個能同時涵蓋上述三種輻射機制的合成模型(synthesis model) 來深入研究在這些 X 射線噴流中，不同輻射機制所占的組成比例與其物理參數。從我們的分析顯示，在目前已知皆有電波、可見光、及 X 射線輻射的噴流中，SSC 機制似乎爲主導光學波段的輻射來源，而 X 射線卻主要源自於 IC/CMB 機制。利用這些數據以及合成模型，噴流物理環境中的都普勒因子與磁場的可能範圍可進一步被縮小。此外，藉由其他觀測所獲得的束射因子（beaming factor），我們也對部分噴流的能量傳播問題進行一些討論。我們發現同步加速輻射強度隨著遠離活躍星系核而遞減至離核心約 100 kpc 處；然而以 SSC 爲主的輻射源數量卻在此處達到峰值。這可能是第一個指出 X 射線噴流傳播距離極限的證據。

A Multi-wavelength Study of X-ray Jets in Active Galaxies

Huang Zhen-Yuan[a], Chen Lin-Wen[b]

[a.] Institute of Astronomy & Astrophysics, Academia Sinica

[b.] Department of Earth Sciences, National Taiwan Normal University

Abstract

To probe the high-energy origin of AGN jets, a series of analysis incorporating all available X-ray jet data with a synthesis model are carried out, in which the model includes synchrotron radiation, synchrotron self-Compton emission (SSC), and inverse Compton scattering off CMB photons (IC/CMB) – the main radiation mechanisms of X-ray jets as current consensus suggests. It has been demonstrated that synchrotron-dominated and inverse-Compton-dominated jets can be separated into two groups by

comparison of broadband spectral indices; using the similar technique but with a more sophisticated analysis, we have further estimated the possible contributions respectively from the three mechanisms to the observed fluxes of our samples. Our analysis shows that the SSC mechanism is responsible for most optical emission while the IC/CMB model is the major contributor in X-ray; subsequently, the Doppler boosting factor and magnetic field of jets are constrained by the contribution fractions of the three mechanisms. Moreover, with the constrained beaming factors, the de-projected distance of each sample is calculated to determine the emission nature of jet propagation. There is an interesting trend showing that the synchrotron emission declines out to 100 kpc away from AGN cores and incidentally most of the optical and X-ray emission produced by SSC appears significantly at around the same scale. This could be the first evidence to indicate the average transportation limit of high-energy emission from jets.

關鍵字(Key words)：X 射線噴流（X-ray jets）、活躍星系核（AGN）、輻射機制（radiation mechanisms）

1. Introduction

Since the launch of Chandra X-ray telescope, there are increasing detections of X-ray emission associated with extragalactic radio jets (to date, 75 X-ray jets). The high resolution of Chandra around 0.5 arcsecond is capable to clarify several characteristics of relativistic jets and unsolved problems left from previous X-ray observations. It is generally believed that radio jets consist of ionized particles confined by magnetic field and radiate synchrotron photons which result in the observed steep power-law spectrum. However, a fundamental question regarding that whether the previous model alone can still account for new observed X-ray emission emerges as most sources reveal X-ray excess to the extrapolation of the radio synchrotron spectrum. This concave spectrum somehow implies other components to account for the observed emission in addition to the original synchrotron contribution. The consensus model is inverse Compton scattering mechanism which is sub-divided into synchrotron self-Compton emission (SSC) and inverse Compton scattering off comic microwave background photons (IC/CMB) amplified by jet bulk motion. From a series of studies in recent years, the SSC model in equipartition is favored for un-beamed hotspots in FR II radio galaxies (Hardcastle et al. 2004) and IC/CMB mechanism is suggested for the scenario of relativistic jet knots (Sambruna et al. 2004). Among those successfully explained cases, it is still worthy to note that an interesting source, namely 3C 273 (Marshall et al. 2001), which has decreasing X-ray brightness along the extended jet from nuclei while the radio emission shows a

totally inverse trend. Such an anti- correlation between radio and X-ray emission leaves more space for further investigation on jet physics (e.g. trans-portation of jets) apart from the framework of the X-ray models mentioned above.

Following the physical condition inferred from these X-ray models, including synchrotron, SSC, and IC/CMB, the associated physical parameters can be investigated for detailed understanding of X-ray jets. The most important one is the correlation between magnetic field and Doppler boosting factor (e.g. Tavecchio et al. 2000; Dermer & Atoyan 2004). It has been narrowed down to predict the local condition of X-ray jets with B field in the range of micro-Gauss to mini-Gauss and the Doppler factor from unity to few tens.

Although several observed results can be accounted for by a single X-ray mechanism, uncertainties of physical parameters usually still remain and the values are model-dependent. To interpret such excess emission and constrain the X-ray properties in more detail, we present a study with a synthesis model (Fig. 1) involving three consensus mechanisms for pursuing more intrinsic jet properties and the associated physical conditions.

Based on the analysis of our synthesis model, the method to decompose the observed flux of selected samples into possible model components is described in Section 2. The statistical results are shown in Section 3. We focus on the preliminary results of different model fractions which are the ratios of predicted emission to observed emission, and discussion on the associated emission mechanism comprehensively. Finally we summarize the properties of X-ray jets derived from our analysis in Section 4. Throughout this work, H_0 = 71 km s^{-1} Mpc^{-1} and q_0 =0.5 are adopted.

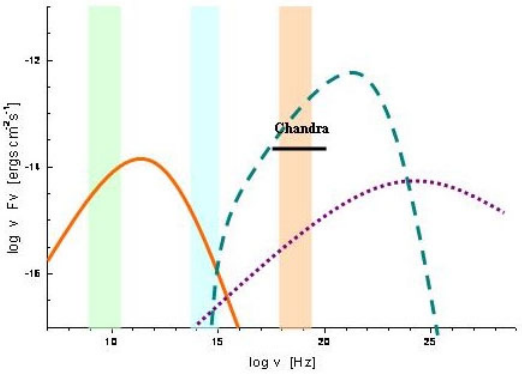

Fig. 1: A schematic diagram of spectral energy distribution of X-ray jets illustrating energy contributed from three model components and the observed frequencies. The solid line represents emissions from synchrotron radiation; dash line shows emissions from IC/CMB process, and the dotted line marks SSC process. The green, blue, and orange bands show the frequency ranges of observations in radio, optical, and X-ray, respectively. In general, extended X-ray jets are observed by Chandra at flux level between 10^{-13} and 10^{-14} ergs cm^{-2} s^{-1}.

2. Analytic Models & Archival Data

2.1. The Synthesis Model

We start our analysis from analytic formulae (Dermer & Atoyan 2004; Dermer et al. 1997). By assuming a spherical blob with radius r_b progressing with bulk Lorentz factor $\Gamma \equiv \left(1-\beta^2\right)^{-1/2}$ and Doppler factor $\delta \equiv \left[\Gamma\left(1-\beta\cos\theta\right)\right]^{-1}$ while an angle exists between the jet and the observer's line of sight, the observed emission can be determined by distinct nonthermal models. The electrons are considered randomly filling the emission region with a typical index p of electron energy distribution in the range of $2<p<3$. Since we have to consider the high-energy loss in synchrotron spectra, the electron distribution within Thomson limit is generalized from a single

power law to a broken power-law with a steeper cooling slope after break point γ_{brk} (e.g. Hardcastle et al 2002):

$$N_e^{'}(\gamma) = N_0 \gamma^{-p}, \quad \gamma_{\min} \le \gamma \le \gamma_{\mathrm{brk}}$$
$$= N_0{}^{'} \gamma^{-(p+1)}, \quad \gamma_{\mathrm{brk}} \le \gamma \le \gamma_{\max}$$
$$=0, \quad \text{otherwise.} \qquad (1)$$

In the radio regime, the only mechanism is synchrotron radiation and the observed spectrum that also appears approximately as a power law ($F_\nu \propto \nu^{-\alpha}$) can be connected with the spectral index α by $p=2\alpha+1$. Using the spectral energy density $f_\varepsilon = \nu F_\nu$, the synchrotron radiation spectrum is approximated by the expression

$$f_\varepsilon^{syn'} = C_1 (1+z)^{1-\alpha} N_0 \delta^{3+\alpha} B^{1+\alpha} \nu^{1-\alpha} \qquad (2)$$

where the coefficient is defined as

$$C_1 = \frac{c\sigma_T}{48\pi^2 d_L^2} \left(\frac{hB_{cr}}{m_e c^2} \right)^{1-\alpha} \qquad (3)$$

$\sigma_T = 6.65\times10^{-25} cm^2$ is Thomson cross section, and B_{cr} is critical magnetic field defined by $\frac{2\pi m_e^2 c^3}{eh} = 4.414\times10^{13} G$.

While the old populations of electrons in the emitted volume suffer high-energy losses, the shape of the synchrotron spectrum starts to break and becomes:

$$f_\varepsilon^{syn} = C_2 (1+z)^{(1-2\alpha)/2} N_0 \delta^{(2\alpha+7)/2} B^{(2\alpha+3)/2} \nu^{(1-2\alpha)/2} \qquad (4)$$

where the coefficient is

$$C_2 = \frac{c\sigma_T}{48\pi^2 d_L^2} \left(\frac{hB_{cr}}{m_e c^2} \right)^{(1-2\alpha)/2} \qquad (5)$$

In the scenario of inverse Compton scattering cosmic microwave background (IC/CMB), the source photon energy

$\varepsilon_* = \Gamma \times 2.70 k_B T_{CMB} (1+z) / m_e c^2 = 1.24\times10^{-9} \Gamma (1+z)$

and energy density $u_* = \left(\frac{4}{3} \Gamma^2 \right) 4\times10^{-13} (1+z)^4 \ ergs\, cm^{-3}$ are adopted with corrections of moderate Doppler boosting (e.g. Harris & Krawczynski 2002). Thus the high-energy emission is

$$f_\varepsilon^{CMB} = C_3 (1+z)^4 N_0 \delta^{4+2\alpha} \Gamma^{1+\alpha} \nu^{1-\alpha} \qquad (6)$$

where the coefficient

$$C_3 = \frac{8\times10^{-13} c\sigma_T}{9\pi d_L^2} \left(\frac{h}{2.48\times10^{-9} m_e c^2} \right)^{1-\alpha} \qquad (7)$$

For a synchrotron self-Compton (SSC) spectrum, the inverse Compton scattered emission through delta-function approximation is

$$f_\varepsilon^{SSC} = C_4 (1+z)^{1-\alpha} N_0^2 \delta^{3+\alpha} B^{1+\alpha} \nu^{1-\alpha} \qquad (8)$$

where the coefficient

$$C_4 = \frac{c\sigma_T^2}{96\pi^3 d_L^2 r_b^2} \left(\frac{hB_{cr}}{m_e c^2} \right)^{1-\alpha} \Sigma_C \qquad (9)$$

The Compton-synchrotron logarithm in C_4 is defined as $\Sigma_C = \ln\left[\frac{\min(\varepsilon_B \gamma_{\max}^2, \varepsilon^{'} / \gamma_{\min}^2, \varepsilon^{'-1})}{\max(\varepsilon_B \gamma_{\min}^2, \varepsilon^{'} / \gamma_{\max}^2)} \right]$ with $\varepsilon^{'} = (1+z)\varepsilon/\delta$. A nominal and frequency independent Σ_C of 10 is assumed in this paper (Dermer & Atoyan 2004).

A schematic spectral energy distribution of a jet shown in Fig. 1 demonstrates how the integrated emissions of the three mechanisms are responsible for the observed flux from low to high-energy bands. It is quite different from previous investigations that usually applied one individual model exclusively with its associated physical parameters to data.

By applying Eqs. 2 – 9 to observed data, one can simultaneously estimate the possible contributions from the three main radiation mechanisms and even constraints on the physical condition of the jets. In Fig. 2, the observed spectral energy density (3×10^{-15} erg cm^{-2} s^{-1} at 4.8 GHz and 1.9×10^{-14} at 1 keV, see Chartas et al. 2000) of knot WK7.8 of PKS 0637-752 is compared with the model-predicted emission (the bottom panels) as a function of magnetic field B, in which several

Fig. 2: Model fractions as a function of B field with assumed electron numbers N_0 (10^{60} and 2×10^{63} respectively in left and right columns) in a 1 kpc radius emitting blob. The first two rows are the predicted emission components due to synchrotron radiation, external mechanism by CMB photons, and SSC emission represented by solid, dotted, and dashed lines respectively (see Eqs 2 – 9). Each individual model is normalized by the total model flux; thus the dominant mechanism and associated physical parameters can be constrained by fitting to the observed flux fractions (see Fig. 4 below). In the bottom panels, radio synchrotron radiation (dashed line) and sum of three predicted model emissions in X-ray (solid line) are plotted for comparison with model fractions above. Some parameters are taken from the observed values of knot WK7.8 of PKS 0637-752 (see texts for detail).

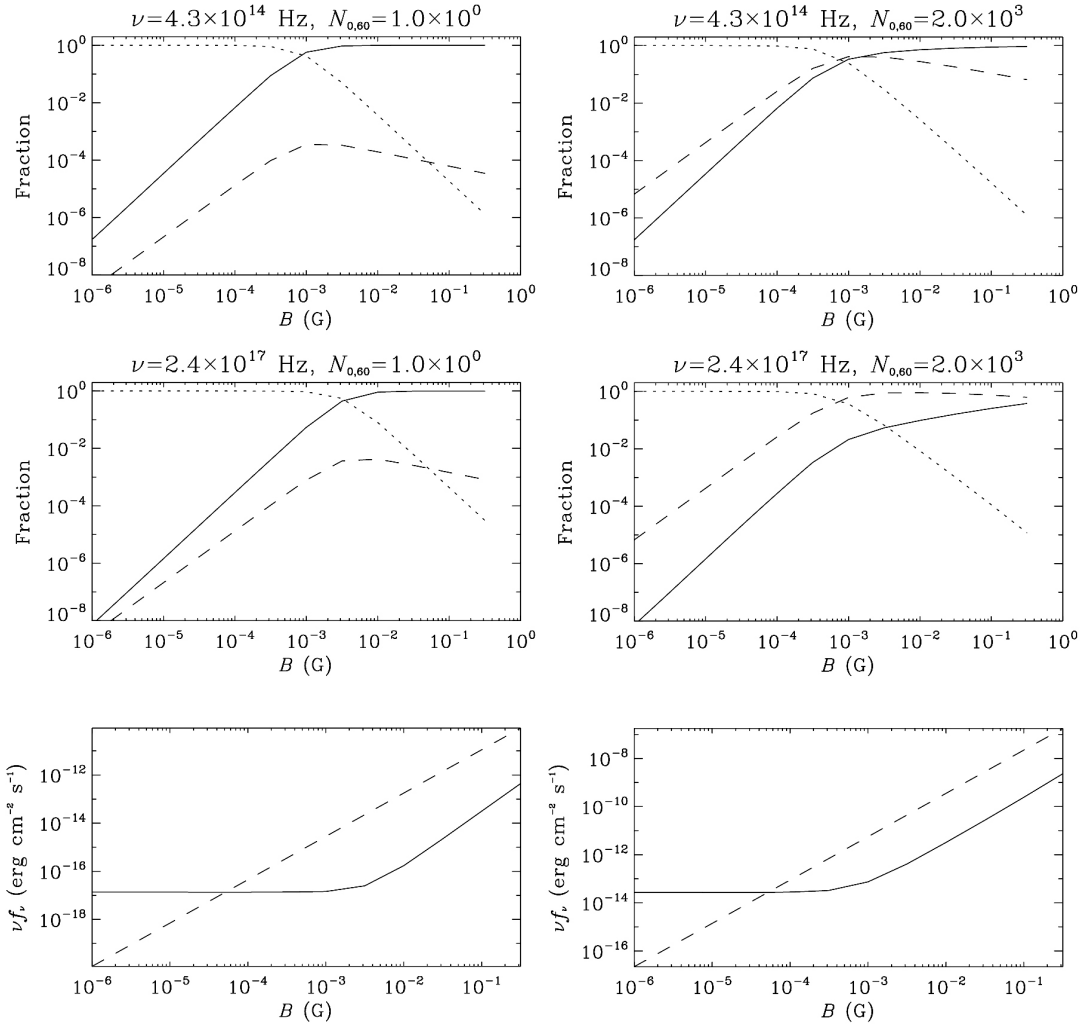

observed parameters of the knots are fixed or assumed, including electron number N_0 (10^{60} and 2×10^{63} for right and left panels), redshift z=0.651, electron distribution index p=2.6, Doppler factor δ=5, Lorentz factor Γ=2, and the radius of emitting region r_b=1 kpc; meanwhile the top and middle panels show the fractional composition of the three radiation components. As indicated by the right-bottom plot in Fig. 2, the observed flux of the knot favors a physical condition of magnetic field ~ few tens of micro-gauss, which implies the dominant contributor is IC/CMB photons (see the right-middle panel). This is consistent with previous results of the X-ray jets originated from CMB process (e.g. Tavecchio et al. 2000). On the other hand, if a smaller electron number is chosen (N_0 =10^{60} in the left column), there is no coherent solution for B. In this paper, we focus on analysis of model fractions only, a detailed study on the physical properties of jets derived from model

fractions will be reported in Huang & Chen (2006).

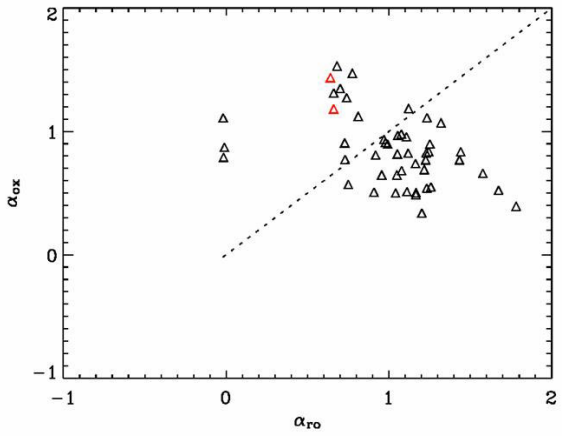

Fig. 3: Spectral indices α_{ox} versus α_{ro}. The dashed line represent the locus where $\alpha_{ox} = \alpha_{ro}$. Above the dashed line, the SED is the convex spectrum which is suggested for synchrotron X-ray emission. Below the dashed line, the concave spectrum population is dominant, so the other mechanism is needed to interpret excess X-ray emission. The synchrotron-preferred ($f_{syn} \geqq 0.4$) sources in this analysis are denoted by red triangles.

2.2. Selected Criteria of Jet Samples

Fifty-four samples with available radio-optical-X-ray continuum data are selected for model fitting, and respective contributions of the three models to the observed flux are obtained. The correlation of broadband indices (radio-optical & optical-X-ray) of our sample is first compared for preliminarily determining dominant mechanism as shown in Fig. 3. The dashed line separates two populations: a convex spectrum responds to synchrotron in the upper-left space and concave spectrum is related to inverse Compton mechanism in the lower-right space. Our sample is consistent with previous study by Sambruna et al. (2004) who showed that most X-ray jets need high-energy photons resulted from Comptonism. However, how to determine the dominant mechanisms, including SSC and IC/CMB, for X-ray emission is not understood yet in this comparison. Therefore, we use the synthesis model to analyze possible models which can produce observed emission and discuss a few corresponding important issues.

3. Results & Discussion

3.1. Fraction distributions of Model Components

The distributions of model fractions (Fig. 4) reveal important messages about the dominant mechanisms in a wider scope by comparing with Fig. 2. Our results show synchrotron radiation is lightly weighed in high-energy regime and contributes less observed emission in X-ray than optical. Therefore the excess spectra are attributed to two inverse Compton mechanisms: SSC accounts for most optical components while IC/CMB is responsible for producing main X-ray emission. We also note that all observed X-ray jets have stronger flux (νf_{ε}) in X-ray than that in optical, which implies that the magnetic field in these sources must be sub-mini-gauss (see plots in the bottom raw of Fig. 2).

Moreover, if combined with another result of IC/CMB and SSC respectively being the primary and secondary mechanism to produce X-rays for most sources (result from Fig. 4), then our analysis suggests further that the electron number in a typical volume (~1 kpc) of jets is greater than 10^{63} (see the 2 figures in the middle raw of Fig. 2 for a comparison). From these relations, it can be concluded that nature of optical emission is strongly influenced by the extended spectrum of radio synchrotron flux; nonetheless the X-ray

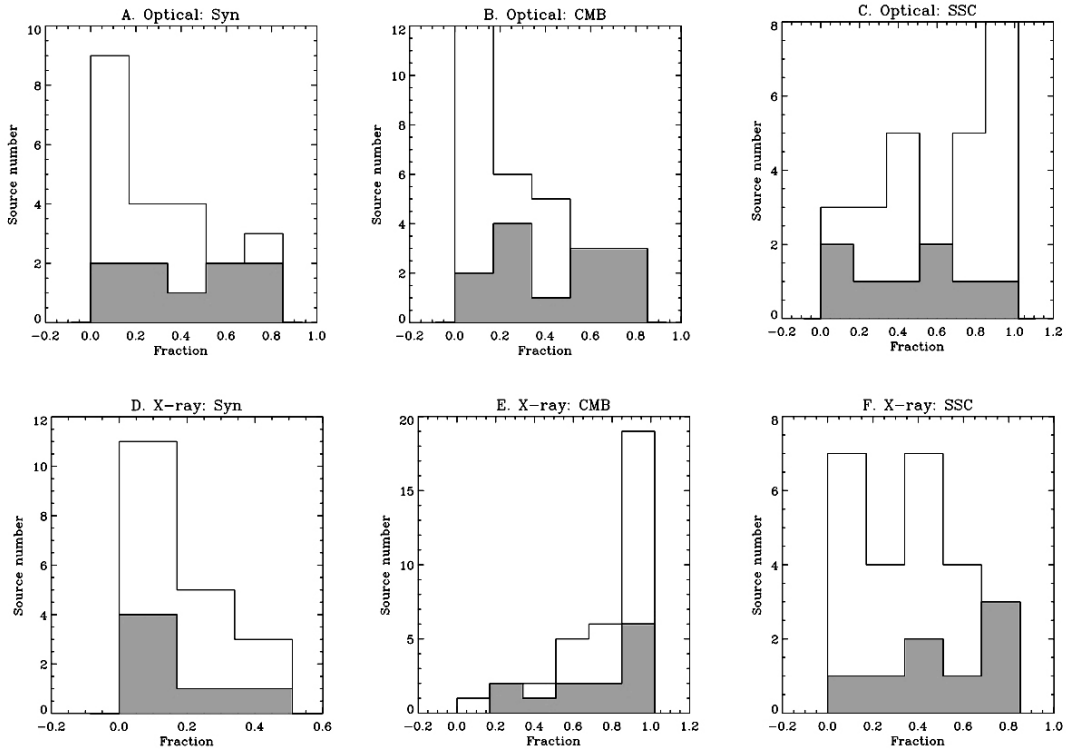

Fig. 4: Histograms of the fraction distribution of three model components both in optical and X-ray bands are presented. Grey regions represent samples which have total fractions (predicted model emission divided by observed emission) larger than 0.7 in both optical and X-ray.

regime requires external components other than synchrotron for producing high-energy emission. On the other hand, except the samples marked in yellow which are better interpreted in optical and X-ray (total fraction $\geqq$ 0.7), many samples still have energy flux of unknown origins. There is almost no obvious trend in the yellow sub-samples especially at optical wavelength, while high-energy IC/CMB and SSC mechanisms are still prominent in X-ray.

3.2. Energy Transport from Parsec to Kilo-parsec Scale

Using the beaming factors (Lorentz factor and viewing angle) of 27 samples determined from VLBI observations, we estimate the de-projected distance of jets. Some tendencies of model fractions along jets are discovered as shown in Fig. 5.

Because of the nature of jet deceleration, the efficiency of synchrotron radiation declines as a function of distance to the core and it indicates an energy loss with continually decreasing Lorentz factor. Some main physical parameters with such a decreasing trend, like Doppler factors and magnetic fields, related to synchrotron model are needed. A similar idea has also been proposed by Sambruna et al. (2001) in which one- component synchrotron model is used to interpret the changing emission of knots along the jets in 3C 273.

On the other hand, the IC/CMB model claims the X-ray emitting electrons are in relatively low energy (γ~ a few hundred) and have to be boosted to radiate sufficient observed emission with Γ~10 (Tavecchio et al. 2000). Since

local CMB energy density in the comoving frame should be uniform, following the decreasing Lorentz factor as suggested in synchrotron regime, the IC/CMB component must show a similar tendency but it is not what our results show, as there is no variation of IC/CMB emission along jets in the middle panel of Fig. 5. Thus there should be somehow a parameter playing a crucial role to strengthen the IC/CMB flux along jets.

The astonishing peak of SSC emissions appearing at around 100 kpc (the bottom panel of Fig. 5) could be attributed to jet geometry and related radiative cooling timescales. In collimated jets, besides the decelerating kinetic power, the modified geometry of jets (e.g. a faster spine and a slower sheath) can have significantly different radiative cooling efficiencies (Celotti, Ghisellini, & Chiaberge, 2001), the SSC peak at this limit could be simply due to such efficiency variation with other distance-dependent factors (eg, electron density) incorporated.

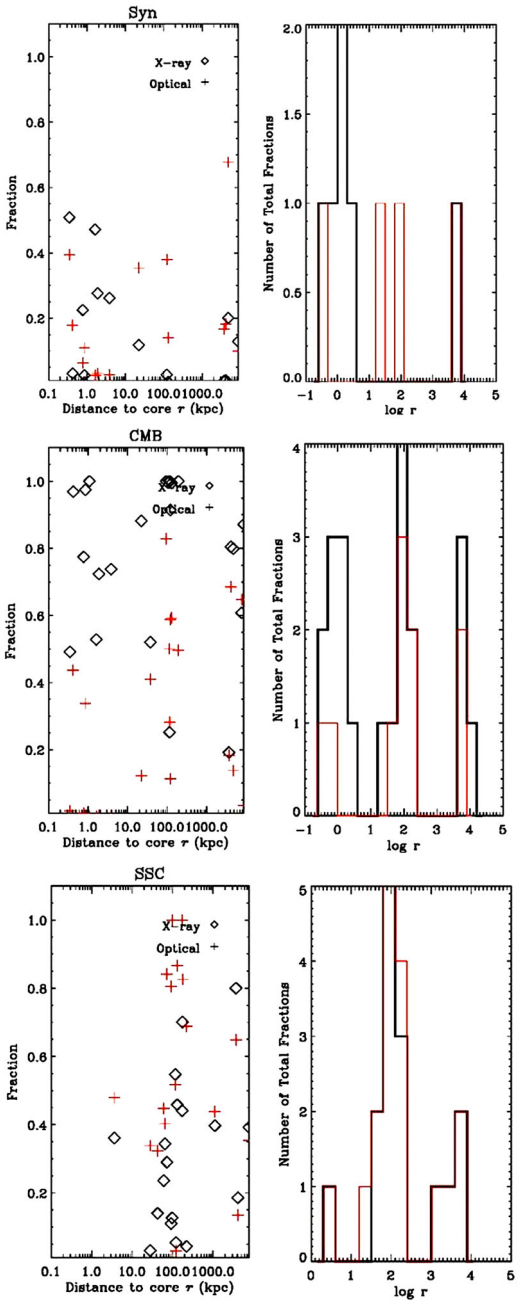

Fig. 5: In the left column, the model fractions (from top to bottom: synchrotron, EC/CMB, and SSC) are shown along the physical distance of every component. In the right column, the fraction number along the increasing distance is counted as histograms.

4. Conclusion

The analysis in this study has estimated the contributions respectively from three main mechanisms in our proposed integrated model for further investigation on detailed physical condition of X-ray jets. Several correlations between the observable quantities and physical parameters are summarized below.

- **SSC favoritism in optical and IC/CMB dominates in X-ray**

Although IC/CMB and SSC models are both suggested for X-ray origin of radio jets, our results shows that the SSC process is vital in optical regime while IC/CMB mechanism dominates the X-ray band. It might just reveal the connection between low-energy and high-energy emissions. Starting from radio synchrotron spectrum in SED, the SSC mechanism continues

to produce synchrotron power by scattering its photons and then the IC/CMB mechanism will take the job for contributing higher energy photons in the jets.

♦ Distance-dependent profile in model fraction

There is a trend of decreasing flux found in synchrotron domain along the jet downward to outermost, and the model fractions congregate around 100 kpc in the SSC domain. Furthermore, no obvious tendency is found in IC/CMB domain. Apart from determination of decreasing bulk Lorentz factor, we suggest other obscure factor to strengthen IC/CMB component and the spine-sheath geometry of jets to account for prominent SSC model fractions due to radiative efficiency along jets.

For a better understanding of the nature of AGN jets, further analysis to derive the values of separated physical parameters will be carried out based on the results of decomposed radiation model components in this study. This should provide more pieces of convincing evidence for correlations reported in this paper, such as those related to the energy transportation issue. Moreover, to generalize our analysis for more broad-band studies of jets, we will build a library of spectral templates to connect the measured model fractions and the fundamental physical properties. This can also help interpret those mysterious sources which are lack of X-ray emission but luminous in optical, or vice versa.

Acknowledgement

HZY thank the support from National Science Council (NSC Undergraduate Research Project 93-2815-C-003-015-M).

References

Celotti, A., Ghisellini, G., & Chiaberge, M. 2001, *MNRAS*, 321, L1

Chartas, G. et al. 2000, *ApJ*, 542, 655

Dermer, C. D., Sturner, S. J., & Schlickeiser, R. 1997, *ApJS*, 109, 103

Dermer, C. D. & Atoyan, A. 2004, *ApJ*, 611, L9

Hardcastle, M. J. et al, 2002, *ApJ*, 581, 948

Hardcastle, M. J. et al. 2004, *ApJ*, 612, 729

Harris, D. E. & Krawczynski, H. 2002, *ApJ*, 565, 244

Huang, Z. Y. & Chen, L.-W. 2006, in preparation

Marshall, H. L. et al. 2001, *ApJ*, 549, L167

Sambruna et al. 2001, *ApJ*, 549, L161

Sambruna, R. M. et al. 2004, *ApJ*, 608, 698

Tavecchio, F. et al. 2000, *ApJ*, 544, L23